Coherent Control of THz Wave Generation in Ambient Air

Xu Xie, Jianming Dai, and X.-C. Zhang*

Center for Terahertz Research, Rensselaer Polytechnic Institute, Troy, New York 12180 USA

(Received 14 December 2005; published 23 February 2006)

Our study of THz wave generation in the pulsed laser induced air plasma with individually controlled phase, polarization, and amplitude of the optical fundamental wave (ω) and its second harmonic (2ω) indicates that the third-order nonlinear optical process mixing the ω and 2ω beams in the ionized plasma is the main mechanism of the efficient THz wave generation. The polarity and the strength of the emitted THz field are completely controlled by the relative phase between the ω and 2ω waves. The measured THz field amplitude is proportional to the pulse energy of the fundamental beam and to the square root of the pulse energy of the second-harmonic beam once the total optical pulse energy exceeds the plasma formation threshold. The optimal THz field is achieved when all waves (ω, 2ω, and THz waves) are at the same polarization in the four-wave-mixing process.

DOI: 10.1103/PhysRevLett.96.075005 PACS numbers: 42.65.Re, 52.38.−r

THz wave generation in ambient air has attracted considerable attention recently [1–7]. The first reported THz wave generation was achieved in the early 1990s by focusing an intense (peak power 10^{12} W) laser beam into air [1,2]. Through the mixing of an optical fundamental wave with its second-harmonic (SH) wave, the generation of intense THz wave pulses in air has been demonstrated [3–5]. Optical power dependence measurements across the air breakdown threshold suggested that the ionized air (plasma) plays an important role in the generation of THz radiation [4,5]. Recently, a THz field strength greater than 100 kV/cm has been reported by using a similar experimental arrangement with shorter optical pulses [7].

In all previous experiments, a thin β-barium borate (BBO) crystal (typically type-I) was placed after the focusing lens in the fundamental beam (ω) path to generate second-harmonic wave (2ω); the 2ω and residual ω beams created plasma at the focus. The different symmetry between the second-order susceptibility tensor $\chi^{(2)}$ for 2ω generation and the third-order susceptibility tensor $\chi^{(3)}$ for THz wave generation causes the optimal angle for THz wave radiation to not follow the optimal angle for the 2ω generation. This may be the source of the inconsistency between the values of the emitted THz field versus the optical excitation energy in previous reports [3,4,7].

In this Letter, we report the systematic study of THz wave generation in air with individually controlled polarization, phase, and amplitude of the fundamental and second-harmonic beams. Our coherent control measurement confirms that the four-wave mixing (FWM) in the air plasma is the major mechanism of THz wave generation. We also prove that the optimal efficiency of the THz field is achieved when all the waves (ω, 2ω, and THz waves) are at the same polarization corresponding to $\chi^{(3)}_{xxxx}$ in the FWM process, while the contribution from $\chi^{(3)}_{xxyy}$ is very small.

We first repeated the THz wave generation following the experiments reported previously by the pioneer groups [1,3,4,7]; typical setups of optical beam excitation in air are schematically illustrated in Figs. 1(a) and 1(b). Figure 1(a) uses a single optical beam excitation, in which the THz wave generation is assigned to the ponderomotive force driving electrons and ions. Figure 1(b) is the common setup for FWM that results from the third-order nonlinear optical process. The ω beam and its 2ω beam generated by a type-I BBO crystal (the thickness of which was varied from 0.1 mm to 2 mm) are focused in air. The optical source is a Ti-sapphire amplified laser (Spectra-Physics Hurricane *i*) with a central wavelength of 800 nm, 140 fs

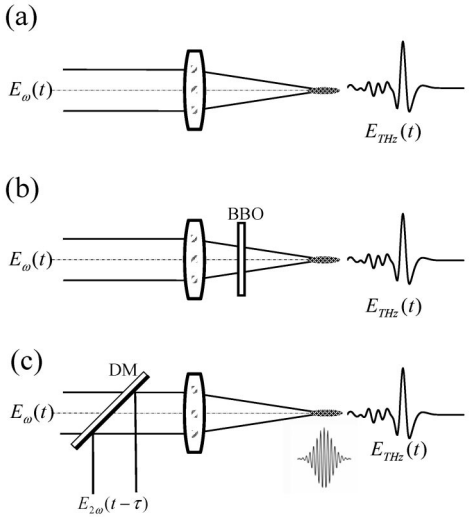

FIG. 1. Three schematic illustrations of the experimental setups. (a) A single optical beam excitation (ω or 2ω), in which the THz wave generation is assigned to the ponderomotive force to drive electrons and ions. (b) The common setup for the FWM which assuming the third-order nonlinear optical process. (c) A dichroic mirror combines the second harmonic beam with the fundamental beam. Phase, amplitude, and polarization of both beams can be controlled individually.

pulse duration, 860 μJ pulse energy and 1 kHz repetition rate. The emitted THz wave was measured by the standard time-resolved electro-optic sampling method with a 3 mm thick $\langle 110 \rangle$ oriented ZnTe crystal [8].

After we duplicated the THz wave generation in air using the previous method, we controlled the phase, polarization, and amplitude of each beam individually. We separated the fundamental beam (ω) and its second-harmonic beam (2ω) by using a dichroic mirror into different optical paths with individual polarizers, attenuators, and a time delay piezoelectric stage with a resolution of 13.6 nm/step (90 attosecond/step). Finally, the two beams are recombined by another dichroic mirror, as shown in Fig. 1(c). A fused quartz lens with a focal length of 200 mm is used to focus the combined beams.

Plots of 3 THz waveforms generated in the air are shown in Fig. 2. The bottom and middle curves are obtained from a single beam (ω and 2ω, respectively) using the geometry shown in Fig. 1(a), and the top curve is obtained from the four-wave-mixing in the geometry of Fig. 1(b). A lower plasma threshold for the THz generation with a single 2ω beam is observed in comparison to a single ω beam, which is consistent with the explanation of ponderomotive force driving the ions and electrons since the short wavelength laser beam has higher confinement at the focal point and hence meets the plasma generation intensity threshold with a lower pulse energy [9].

In the FWM THz rectification process, the frequencies of the three input beams add to nearly zero (THz frequency). When a pulsed laser is used, the nonlinear response is driven by the envelope of the input fields. This envelope composes the rectified field which is the source of the THz wave. Mathematically, this third-order nonlinear process is related with $\chi^{(3)}(\Omega; 2\omega + \Omega, -\omega, -\omega)$, where Ω is the frequency of emitted THz wave. Predicted by the four-wave-mixing theory, the THz field has the form as [3],

$$E_{\mathrm{THz}}(t) \propto \chi^{(3)} E_{2\omega}(t) E^{*}_{\omega}(t) E^{*}_{\omega}(t) \cos(\varphi), \tag{1}$$

where $E_{2\omega}(t) = 1/2 E_{400} \exp(i2\omega t) + \text{c.c.}$, $E_{\omega}(t) = 1/2 E_{800} \exp(i\omega t) + \text{c.c.}$, and the phase factor $\phi = k_{2\omega} \Delta l$ is the relative phase difference between the ω and 2ω beams, with $k_{2\omega}$ being the wave vector of the 2ω beam and Δl being the path difference between the ω and 2ω beams along the beam propagation direction. If the ω and 2ω beams propagate along different paths before they are recombined, as shown in Fig. 1(c), the relative phase has the form $\varphi = k_{2\omega} \Delta l = \omega_{400} \tau$. In this way, φ can be controlled arbitrarily by changing the beam path difference, Δl. Equation (1) is based on the plane-wave approximation. When a lens with a short focal length is used before the BBO crystal, an additional phase correction term is required to include the angle-dependent dispersion between the ω and 2ω beams at the air-lens interfaces. In previously reported methods, φ can be determined by the dispersion of the ω and 2ω beams in air since they travel the same distance to the focal point. When describing the THz field as a function of optical beam power, Eq. (1) can also be written as

$$E_{\mathrm{THz}} \propto \chi^{(3)} \sqrt{I_{2\omega}} I_{\omega} \cos(\varphi). \tag{2}$$

If the nonlinear media is spatially isotropic, there are three independent components in the third-order susceptibility tensor: $\chi^{(3)}_{xxxx}$, $\chi^{(3)}_{xyxy}$, and $\chi^{(3)}_{xxyy}$, with the four subscripts corresponding to polarizations of Ω, 2ω, ω, ω beams, respectively.

The emitted THz wave is measured by scanning the probe beam time delay, which is the basic concept behind THz time domain spectroscopy. When the timing between the one of the pump beams (ω or 2ω) and probe beams on the ZnTe detector is set at the peak (maximum signal) and the phase φ between the ω and 2ω beams is scanned by changing Δl, modulation of the THz wave is expected because the amplitude the THz wave is proportional to the product of fields of the ω and 2ω beams. A type-I BBO crystal has its maximum conversion efficiency when the polarization of the ω beam is perpendicular to the e axis and the polarization of the generated 2ω beam is parallel to the BBO's e axis. The 2ω beam and the ω beam will have their polarization perpendicular to each other [10].

In our experiment, the azimuthal angle of the BBO crystal is fixed such that the maximum 2ω beam is generated. Our electro-optic detection geometry measured only the p-polarized THz wave. By adjusting the half-wave plates in the ω and 2ω beam paths, we observed different amplitudes and polarizations of THz wave. Figure 3 plots eight waveforms with combinations of the polarizations of the four waves. When both the ω and 2ω beams are p polarized, the emitted THz wave has maximum amplitude in p polarization which corresponds to $\chi^{(3)}_{xxxx}$, as shown in the top trace ($xxxx$) in Fig. 3. Because of

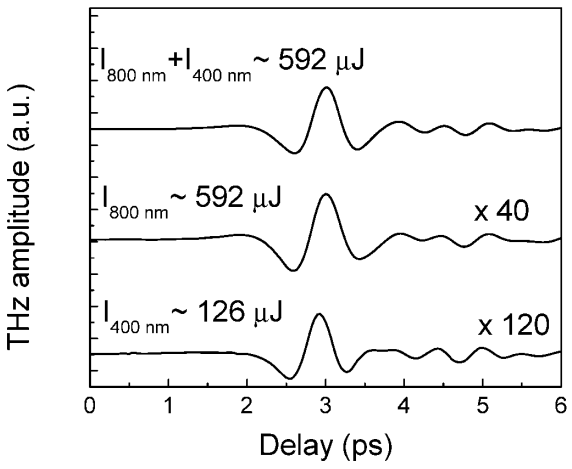

FIG. 2. THz waveforms obtained by (a) focusing the ω and 2ω beams in air, (b) and (c) by focusing a single beam in air (ω or 2ω), respectively. The detection is standard electro-optic sampling method with a 3 mm thick ZnTe crystal.

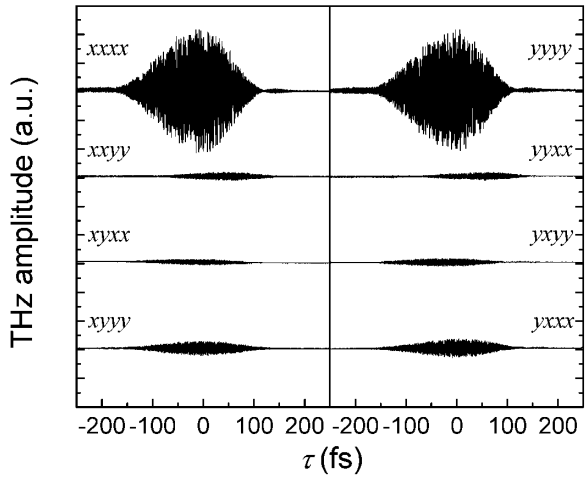

FIG. 3. Interference pattern of rectified field measured by THz pulse peak amplitude from different combinations of polarization of the ω and 2ω beams. The four letters in $\chi^{(3)}$ subscripts represent the polarization of THz wave, the 2ω wave, and the two of ω waves, respectively, in which x corresponds to p polarized and y corresponds to s polarized.

the symmetry, $\chi^{(3)}_{xxxx} = \chi^{(3)}_{yyyy}$, $\chi^{(3)}_{xxyy} = \chi^{(3)}_{yyxx}$, $\chi^{(3)}_{xyxx} = \chi^{(3)}_{yxyy}$, and $\chi^{(3)}_{xyyy} = \chi^{(3)}_{yxxx}$ the measured interference patterns (left and right) in Fig. 3 are equivalent. The second derivative of the envelope of the interference pattern gives the far field THz waveform. The second trace ($xxyy$) in Fig. 3 represents the contribution from $\chi^{(3)}_{xxyy}$. The measurement indicates that this term is small, on the order of $\chi^{(3)}_{xyxx}$, which should be zero in a perfect central symmetric media. We notice that the last trace ($xyyy$) which corresponds to $\chi^{(3)}_{xyyy}$ is not consistent with the zero susceptibility tensor element of an isotropic media, which predicts that both s-polarized ω and 2ω beams should not generate a p-polarized THz wave. This inconsistency may come from the spatial asymmetry of laser induced plasma.

To show the coherent nature of the beam control, Fig. 4(a) plots the partial interference pattern of the first trace in Fig. 3 with a 4 fs temporal window. The solid curve is a fit by an oscillation with 400 nm wavelength. The interference pattern precisely follows the theoretical predication by $\cos(\varphi) = \cos(k_{2\omega}\Delta l) = \cos(\omega_{400}\tau)$ in Eq. (1).

The THz field polarity can be controlled by changing the phase between ω and 2ω beams. When the relative path between the ω and 2ω beams was changed by 200 nm (corresponding to 667 attosecond phase shift for $\phi = \pi$) and the probe beam was scanned, far field THz field waveforms with opposite polarity are obtained, as shown in Fig. 4(b).

Four-wave-mixing theory predicts $E_{\mathrm{THz}} \propto \chi^{(3)}\sqrt{I_{2\omega}}I_{\omega}\times \cos(\varphi)$. Since our experimental arrangement permits us to adjust the power of ω and 2ω beams individually, direct measurements of the emitted THz field amplitude versus each beam's energy are performed, as shown in Figs. 5(a) and 5(b). Here, the THz amplitude (y axis) is the maximum amplitude of the interference data. The power of 1 beam was fixed while the power of other beam was changed. As predicted by the FWM rectification theory, the emitted THz field is proportional to the pulse energy of the ω beam and the square root of that of 2ω beam.

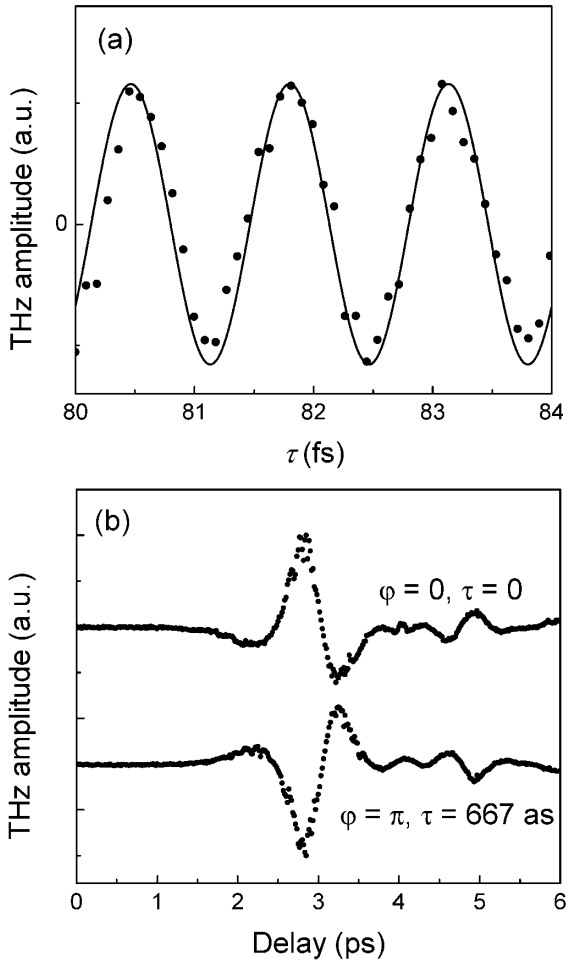

FIG. 4. (a) The interference pattern with a fine temporal resolution. The curve is a fit by $\cos(k_{2\omega}\Delta l) = \cos(\omega_{400}\tau)$ with 400 nm wavelength. (b) The relative phase between the ω and 2ω beams is changed by π ($\Delta l = 200$ nm), and thus the waveforms show opposite polarity. The THz peak signal is extremely sensitive to the phase; the noise of the peak signal is from the phase fluctuation.

Our experimental results confirm that the threshold of THz wave generation is related to the air ionization threshold. We observed a turning point around 150 μJ (combined pulse energy of ω and 2ω beams) in Fig. 5(a). This is explained by the four-wave-mixing process in the plasma when the laser pulse energy exceeds the air ionization threshold. By considering the combination of different wavelength laser beams, we estimated the power density of 1.5×10^{14} W/cm^2 assuming the focal spot with 30 μm in diameter; this number is consistent with previous reports [4]. Meanwhile, using the standard value of air $\chi^{(3)}$ with

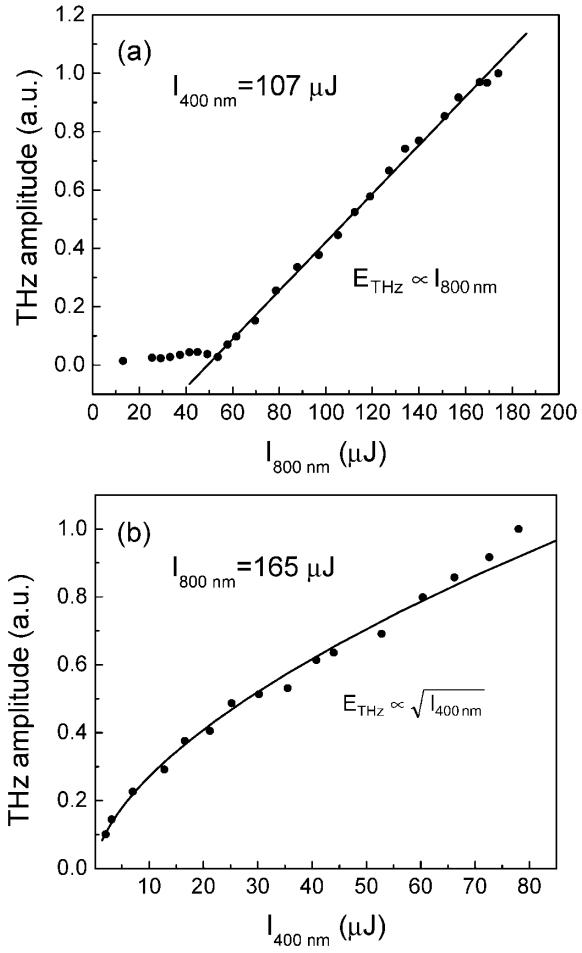

FIG. 5. Dependence of THz amplitude on the power of the (a) ω and (b) 2ω beams. The solid line and curve are the linear fit and the square-root fit, respectively. Once the plasma is created, the THz wave signal follows the equation $E_{\mathrm{THz}} \propto \chi^{(3)}\sqrt{I_{2\omega}}I_{\omega}\cos(\varphi)$.

the 1.5×10^{14} W/cm^2 laser power intensity [10], the calculated THz field is about four orders smaller than our measured field. This behavior reveals the laser induced plasma with a greatly enhanced $\chi^{(3)}$ is the nonlinear media in which the THz wave is generated.

In conclusion, we demonstrated that the four-wave-mixing rectification in the laser induced plasma is the main mechanism of the THz wave generation in the air plasma through the use of individual control of the ω and 2ω beams. The polarity and the strength of the emitted THz field are completely controlled by the relative phase between the ω and 2ω waves. The measured THz field amplitude is proportional to the pulse energy of the ω beam and the square root of the pulse energy of the 2ω beam once the total optical pulse energy is beyond the plasma formation threshold. The optimal efficiency of the THz field generation is achieved when all the waves (ω, 2ω, and THz waves) possess the same polarization in the FWM process. Finally, it is worth pointing out that if we switch the order of the THz field and the second-harmonic field in the third-order susceptibility in the four-wave-mixing optical process, it should be possible to measure the THz wave by using the air as a nonlinear sensor. In fact, the inverse process of FWM in the central symmetric materials, such as silicon and liquids, for the detection of free space THz pulse has been demonstrated [11,12].

We gratefully acknowledge Dr. Jingzhou Xu and Tao Yuan for useful discussion. This work is supported by Army Research Office and the National Science Foundation.

*Email address: zhangxc@rpi.edu

[1] H. Hamster, A. Sullivan, S. Gordon, W. White, and R. W. Falcone, Phys. Rev. Lett. **71**, 2725 (1993).
[2] H. Hamster, A. Sullivan, S. Gordon, R. W. Falcone, Phys. Rev. E **49**, 671 (1994).
[3] D. J. Cook and R. M. Hochstrasser, Opt. Lett. **25**, 1210 (2000).
[4] M. Kress, T. Löffler, S. Eden, M. Thomson, and H. G. Roskos, Opt. Lett. **29**, 1120 (2004).
[5] T. Löffler, M. Kress, M. Thomson, and H. G. Roskos, Acta Phys. Pol. A **107**, 99 (2005).
[6] W. P. Leemans, C. G. R. Geddes, J. Faure, Cs. Toth, J. van Tilborg, C. B. Schroeder, E. Esarey, G. Fubiani, D. Auerbach, B. Marcelis, M. A. Carnahan, R. A. Kaindl, J. Byrd, and M. C. Martin, Phys. Rev. Lett. **91**, 074802 (2003).
[7] T. Bartel, P. Gaal, K. Reimann, M. Woerner, and T. Elsaesser, Opt. Lett. **30**, 2805 (2005).
[8] Q. Wu, M. Litz, and X.-C. Zhang, Appl. Phys. Lett. **68**, 2924 (1996).
[9] T. X. Phuoc, Opt. Comm. **175**, 419 (2000).
[10] Robert W. Boyd, *Nonlinear Optics* (Academic, New York, 1992).
[11] A. Nahata and T. F. Heinz, Opt. Lett. **23**, 67 (1998).
[12] D. J. Cook, J. X. Chen, E. A. Morlino, and R. M. Hochstrasser, Chem. Phys. Lett. **309**, 221 (1999).